7-6

A Novel Full-Band Monte Carlo Device Simulator with Real-Space Treatment of the Short-Range Coulomb Interactions for Modeling 4H-SiC Power Devices

Chi-Yin Cheng
School of Electrical, Computer and Energy Engineering
Arizona State University
Tempe, AZ 85287-5706, USA
chi-yin.cheng@asu.edu

Dragica Vasileska
School of Electrical, Computer and Energy Engineering
Arizona State University
Tempe, AZ 85287-5706, USA
vasileska@asu.edu

***Abstract*—In this work, we present a novel full-band Monte Carlo device simulator for modelling 4H-SiC Power electronic devices in which, for the first time, we use real-space molecular dynamics approach for the Coulomb interactions. Proper treatment of the electron-electron interactions is critical for modelling power electronic devices because of the high electron densities. In addition, because of the high applied voltages, the use of a full-band Monte Carlo device simulator is a must. The simulator has been successfully used to explain the steady-state behavior of a 3-D vertical double-diffused MOSFET (VDMOS) fabricated in the 4H-SiC technology.**

Keywords—4H-SiC, full-band device simulator, vertical double-diffused MOSFET (VDMOS), Monte Carlo Method, real-space treatment of Coulomb interactions.

I. INTRODUCTION

4H-SiC has been widely used in many applications. All of these benefits come from its extremely high critical electric field and good electron mobility [1][2]. 4H-SiC possesses a critical field ten times higher than that of Si, which allows high-voltage blocking layers composed of 4H-SiC to be approximately a tenth of the thickness of a comparable Si device. This reduces the device on-resistance and power losses while maintaining the same high blocking capability [3]. To develop better 4H-SiC devices, good understanding of the transport properties of SiC material is needed and using simulations one can investigate their potential at a low cost. For example, a thorough study of the role of interface traps and self-heating effects on the operation of the SiC power VDMOS device has been performed in [4] and [5]. These authors use technology for computer-aided design (TCAD) tool Silvaco Atlas [6]. Recall that most of the 4H-SiC devices used today are for power electronic applications and are operated under high-voltage conditions. Besides this, the 4H-SiC is an anisotropic material, which features different energy–momentum dispersion profiles along different crystallographic directions. Hence, the drift-diffusion model cannot describe the high-energy behavior of the electron transport precisely. Also, considering the high electron densities in some applications, the impurity scattering issue must be treated properly. In this work, the Coulomb scattering is included via the real-space molecular dynamics (MD) approach. This includes the electron–electron and electron–ion interactions. The molecular dynamics approach is coupled with a full-band ensemble Monte Carlo (FBEMC) simulation framework for the first time. The approach is then used in the simulation of a vertical double-diffused metal-oxide-semiconductor field-effect transistor structure (VDMOS).

II. THEORATICAL MODEL

A. Band Structure Calculation

The first and the critical step in the development of a full-band Monte Carlo transport simulator is the calculation of the band structure. In this work, the empirical pseudopotential method is used. Ng [7] applied a genetic algorithm to find the optimal pseudopotential parameter set for the band structure calculation. The parameter set they proposed is used in this work to reproduce the band structure. The lattice constants used in these calculations are $a = 3.032$ Å and $c = 9.928$ Å, and the bond length is $L_z = 1.866$ Å. The irreducible 1st Brillouin zone is discretized into 21000 $\boldsymbol{k}$-points and all 527 energy levels are calculated.

B. Phonon Scattering Models

Dominant scattering mechanisms in 4H-SiC material system are acoustic phonon, non-polar optical phonon, polar optical phonon and Coulomb scattering. Hjelm [8] presented a complete set of parameters describing the phonon scattering mechanisms in 4H-SiC that are used in this work. The phonon scattering rates are pre-calculated and stored to save run-time execution.

C. Impurity Scattering Model

There are two ways to incorporate Coulomb interaction in particle-based device simulations. The first approach is to include Coulomb scattering in **k**-space. There are several shortcomings to this approach. First, it is difficult to calculate Debye screening length in the case of an inhomogeneous electron gas. Second, it is only valid for binary collisions; the model ignores scattering from multiple impurities at the same time under heavy doping conditions. Third, this scattering approach model assumes that the scattering is instantaneous, and as such, cannot describe the interactions correctly in real space and time domain. Fourth, in power electronic devices electron-electron interaction play very important role and must be accounted for. For the importance of the short-range electron-electron and the electron-plasmon interactions, see the work of Fischetti [9] and Wordelman [10]. To solve most of the above-mentioned difficulties, a real-space molecular dynamics (MD) approach is preferable and is, therefore, adopted in this work. In a real-space Coulomb interaction calculation approach: (1) the non-uniformity in doping is no longer a problem; (2) simultaneous scattering from different impurities is automatically included; (3) the dynamical screening of the Coulomb interaction is also automatically included. Yet, the drawback of the real-space treatment is the calculation time and the scaling ability. The needed time increases dramatically once more particles are considered. To

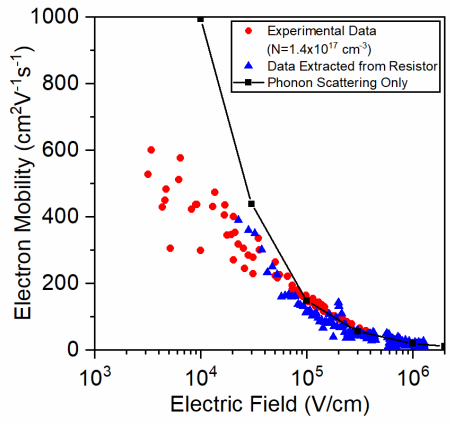

Fig. 1 Comparison of experimental and simulated electron mobility data. Simulation data are extracted from resistor simulations [13]. Also shown here is the phonon-limited mobility (solid black curve). Note that inclusion of the real-space Coulomb interactions accurately describes the field-dependent mobility, in particular at low electric fields, where the importance of this scattering mechanism is most significant. Experimental data are taken from [14].

alleviate the calculation time, the particle-particle-particle-mesh (P^3M) method is used. The concept of the P^3M method is to decompose the interparticle force into two parts: the short-range portion, which is calculated directly from the superimposed Coulomb forces between particles; and the mesh part (called also the Hartree potential), which is calculated through a particle-mesh coupling. Recall that the Coulomb force between two charges is inversely proportional to the square of the distance between them. Hence, for a particle pair, if the distance between them is larger than the threshold, the short-range force calculation can be neglected thus reducing the execution time. To avoid double counting of the mesh force in the short-range region, a reference force is taken from the exact Coulomb force. For a uniform mesh, Hockney and Eastwood [11] proposed that the reference force transitioning smoothly from short range to long range can be described by a sphere with uniformly decreasing density profile *S(r)*. Wordelman [10] modified this approach for the non-uniform mesh case. If the particle pairs are too close, the extremely high and unphysical electric fields must be modified [12]. Otherwise they lead to trapping of the particles (for oppositely charged donors and electrons in the contact region of the device). As adopted in [12], the electric field along a distance shorter than a cut-off range is modified to be linearly decreasing to zero. A cut-off range equal to 1 nm is used in this work.

The details of the methodology for real-space treatment of the Coulomb interaction can be found in [13]. The impact of the Coulomb scattering is illustrated in Fig. 1. The phonon-limited electron mobility along [0001] direction is compared to the data extracted from the example resistor and the experimental data [14]. The doping concentration of the experimental data is $N_d = 1.4 \times 10^{17}\ cm^{-3}$. From the results presented, it is obvious that the inclusion of Coulomb scattering is needed to match the experimental mobility data.

D. Surface Roughness Scattering

Surface roughness scattering at the oxide/SiC interface must be considered, since the channel affects the performance of the device significantly. The need for incorporating this scattering process in the theoretical model is supported by the fact that in the fabrication process of 4H-SiC MOSFETs, the oxide layer is formed by the oxidation of the SiC substrate. The oxidation process leaves carbon precipitation on site, thus leading to significant interface roughness. In our work surface-roughness scattering is also included in real space. It is assumed that the electrons have 50% chance of specular reflection and 50% chance of diffusive reflection at the oxide/SiC interface (This ratio is exactly true for the Si/SiO_2 interface). The ratios chosen here are just for proof-of-concept; users can calibrate the values depending on the fabrication procedure and experimental data of the oxidation layer. If diffusive reflection occurs, the reflected angle is randomized and the momentum and the energy are changed accordingly.

III. Device Structure and Simulation Description

A 3-D VDMOS made of 4H-SiC is presented in this work and has the following parameters. The width of the device (into the paper) is only 20 nm to reduce calculation time. The device consists of a thin (40 nm) n^+ substrate layer, on top of which is grown 1.46 μm of n^- drift region. The doping of the n^- drift layer is $5 \times 10^{16}\ cm^{-3}$. The p well is composed of two parts. The p^- region provides low threshold voltage V_{th} and has doping of $1 \times 10^{17}\ cm^{-3}$; on the other hand, the p region acts as a stopper layer to prevent latch-up, and has higher doping of $5 \times 10^{17}\ cm^{-3}$. The channel length is 0.5 μm (if not mentioned elsewhere) and the oxide thickness t_{oxide} is 0.1 μm. In addition, the doping densities of the n^+ source and drain regions are set to $1 \times 10^{18}\ cm^{-3}$ to ensure good ohmic contacts. The workfunction of the gate contact is set to 4.3 eV. The source contact implemented here has two parts (sections). One section is used for grounding the p^- well; the other one is used for the current path on the top of the n^+ source region. Uniform meshing is used in the simulation of the VDMOS to simplify the Monte Carlo calculation. The charges are coupled to the mesh through the nearest-element-center (NEC) method that eliminates the self-force for the case of materials with different dielectric constants. Note that the non-ideal properties, like traps or defects in the oxide, are important for 4H-SiC devices. They are not included in the present version of the theoretical model. The deviations that they lead to are presently being investigated and the results of these investigations will be published elsewhere. Also, impact ionization, responsible for the breakdown in power converters, at present is not included in the model as well. Furthermore, modifications in the theoretical model to properly account for band crossing [15]–[17] are needed and are currently being implemented in the code.

IV. Simulation Results

A. Electrical Profiles

The example electron and potential profiles for V_G=40 V and V_D=20 V are shown in Fig. 3. Each dot in Fig. 3(a) represents an electron. Since the short-range interparticle force is of interest, the idea of super particle is not adopted in this work.

B. I_D-V_G Transfer Characteristic

I_D-V_G transfer curve is an important characteristic when describing the operation of MOSFET device. To simulate the I_D-V_G curve, usually a small drain bias (< 0.1 V) is applied.

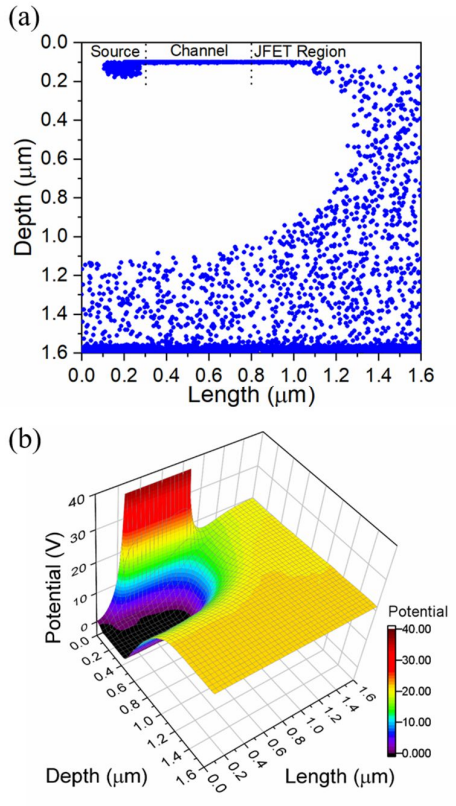

Fig. 3 Electrical profile of example condition. V_G=40 V and V_D=20 V. (a) Electron distribution. Each dot represents an electron. (b) Potential distribution.

Nevertheless, since this voltage level is too small to observe the outcomes in FBEMC device simulations, a voltage V_D=1 V is applied instead. The simulated device parameters are the same as those discussed in the previous section. Fig. 2 shows the I_D-V_G transfer curve of the example VDMOS. Each point is taken as the average of five samples to describe an average device. The threshold voltage V_{th} in this example is about 12 V. It is observed that the drain current I_D gradually gets saturated as V_G > 20 V. This is a typical property of a VDMOS, which is attributed to the high resistivity of the thick and low-doped n^- drift layer, and the parasitic resistance of the JFET region.

C. I_D-V_D Output Characteristic

Fig. 4 depicts the output I_D-V_D characteristic of the device for three gate voltages. The applied gate voltage is taken to be 20 V, 30 V and 40 V. The linear region of the VDMOS is not as obvious when compared to the regular planar MOSFET. In the regular planar MOSFET, the slope of the I_D-V_D curve in the linear region is proportional to V_G-V_{th}. However, this is not the case here because of the limitation of the high series resistances of the drift region and the JFET. Besides this, due to the voltage drop across the resistances, the actual V_D needed to drive the top channel part is less than the drain voltage V_D applied on the electrode. The downward bending of the curves also indicates the presence of the high-resistance drift region. Furthermore, after carriers pass the channel, they change their direction of motion towards the drain. But, since the gate contact is opposite to the drain contact, the increased V_G results in reduced electron velocity

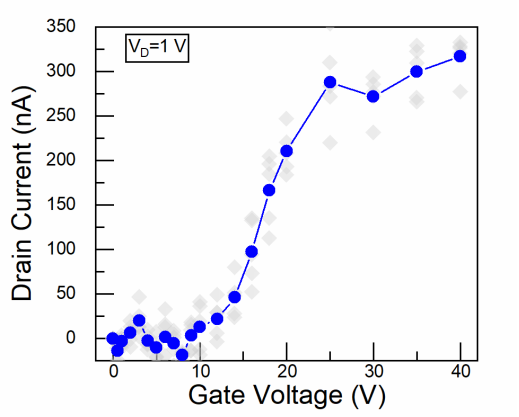

Fig. 2 I_D-V_G transfer curve of the example VDMOS. We use V_D=1 V. Each gray symbol indicates one set of simulation for different distribution of the dopant atoms in the device. (Note that instead of continuum we use atomistic description of the doping.) The blue solid line is the average of the five points of every V_G.

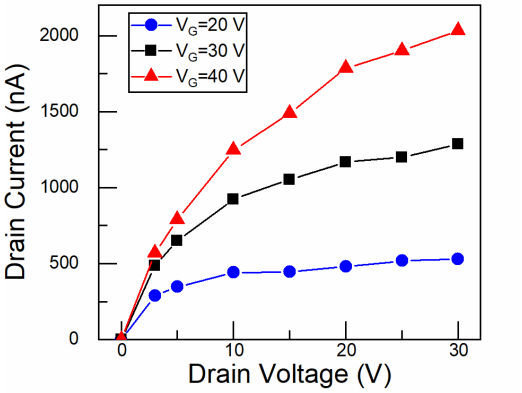

Fig. 4 I_D-V_D (output) characteristics of the example VDMOS. Channel length is 0.5 μm.

when moving toward drain side and, therefore, leads to lower drain current.

D. Channel Length Dependence

Two channel lengths have been investigated in this study. One is the default one (0.5 μm) and the second channel length is taken to be 0.2 μm. The ID-VD curves of the device with channel length $L_{channel}$=0.2 μm are depicted in Fig. 5. Comparing these results to the ones presented in Fig. 4, it is observed that the curves shown in Fig. 5 keep increasing with the increase of the drain voltage. Also, all three curves feature the same slope at high drain voltages. This phenomenon implies that the channel resistance is not dominating anymore. In this case, current is limited by the other resistance components.

E. Temperature Dependence

An obvious advantage of using 4H-SiC is the capability of working under high-temperature environment. Note that the intrinsic carrier density increases exponentially with temperature and is inversely exponentially dependent upon the bandgap. SiC, thanks to its wide bandgap, has intrinsic carrier density much lower when compared to Si or GaAs materials. It is so low that even at high temperature, the

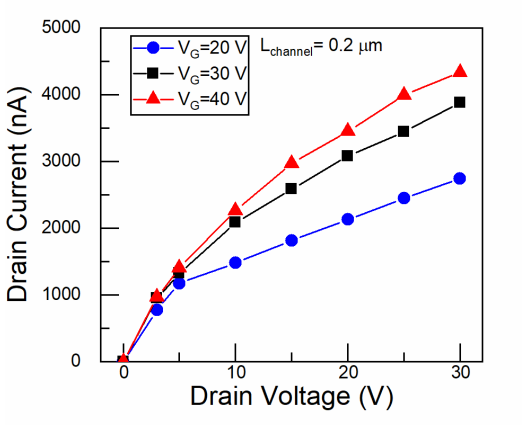

Fig. 5. I_D-V_D output characteristics of example VDMOS. The channel length is 0.2 μm.

concentration of intrinsic carriers is still far lower than of the

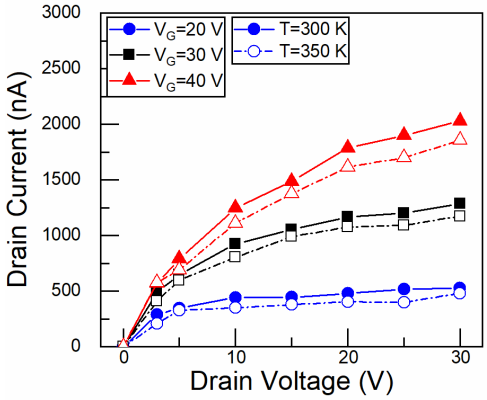

Fig. 6. I_D-V_D output characteristics of the example VDMOS. The channel length is 0.5 μm. Temperature is 300K and 350K.

extrinsic carriers. On the other hand, the concentration of intrinsic carriers in Si or GaAs at high temperature is higher than that of the extrinsic carriers. This results in the malfunction of the device and could damage partially or entirely the system. That is why the temperature dependence is an important characteristic. Fig. 6 shows the temperature dependence. As expected, the currents drop when the temperature is raised to 350 K from nominal 300 K. The degradation of the current is not only attributed to the temperature-related term in the Poisson's equation, but also to the degradation of the mobility resulted from the phonon scattering mechanisms.

V. Conclusion

To explore the performances of a 4H-SiC power devices more comprehensively with low cost, a tool that uses the full-band structure and real-space treatment of the electron–electron and electron–ion short-range Coulomb interactions is needed. The band structure of 4H-SiC was obtained using the EPM. The phonon scattering mechanisms included in our theoretical model are due to acoustic, nonpolar optical, and polar optical phonons. A prototypical 3-D VDMOS is simulated in this work. The simulated I_D–V_G and I_D–V_D curves presented here prove that this device simulator is producing reliable static characteristics. The channel length and temperature dependences are also demonstrated. Since the simulator is particle-based, this provides physical insight not only on the macroscale properties but also the microscale ones. The advantages of this tool lay the foundations for future work on 4H-SiC high power devices. The results of that work will be presented elsewhere.

References

[1] H.Matsunami and T.Kimoto, "Step-controlled epitaxial growth of SiC: High quality homoepitaxy," *Mater. Sci. Eng. R*, vol. 20, no. 3, pp. 125–166, 1997, doi: 10.1016/S0927-796X(97)00005-3.

[2] M.Bhatnagar and B. J.Baliga, "Power Devices," vol. 40, no. 3, 1993.

[3] R.Pérez, D.Tournier, A.Pérez-Tomas, P.Godignon, N.Mestres, and J.Millán, "Planar edge termination design and technology considerations for 1.7-kV 4H-SiC PiN diodes," *IEEE Trans. Electron Devices*, vol. 52, no. 10, pp. 2309–2316, 2005, doi: 10.1109/TED.2005.856805.

[4] M. H.Alqaysi, A.Martinez, K.Ahmeda, B.Ubochi, and K.Kalna, "Impact of interface traps/defects and selfheating on the degradation of performance of a 4H-SiC VDMOSFET," *IET Power Electron.*, vol. 12, no. 11, pp. 2731–2740, 2019, doi: 10.1049/iet-pel.2018.5897.

[5] G. D.Licciardo, S.Bellone, and L. DiBenedetto, "Analytical Model of the Forward Operation of 4H-SiC Vertical DMOSFET in the Safe Operating Temperature Range," *IEEE Trans. Power Electron.*, vol. 30, no. 10, pp. 5800–5809, 2015, doi: 10.1109/TPEL.2014.2376778.

[6] Silvaco TCAD. Available: https://www.silvaco.com/.

[7] G.Ng, D.Vasileska, and D. K.Schroder, "Empirical pseudopotential band structure parameters of 4H-SiC using a genetic algorithm fitting routine," *Superlattices Microstruct.*, vol. 49, no. 1, pp. 109–115, 2011, doi: 10.1016/j.spmi.2010.11.009.

[8] M.Hjelm, H. E.Nilsson, A.Martinez, K. F.Brennan, and E.Bellotti, "Monte Carlo study of high-field carrier transport in 4H-SiC including band-to-band tunneling," *J. Appl. Phys.*, vol. 93, no. 2, pp. 1099–1107, 2003, doi: 10.1063/1.1530712.

[9] M.V.Fischetti, "Effect of the electron-plasmon interaction on the electron mobility in silicon," *Phys. Rev. B. Condens. Matter*, vol. 44, no. 11, p. 5527, 1991, doi: 10.1103/PhysRevB.44.5527.

[10] C. J.Wordelman and U.Ravaioli, "Integration of a particle-particle-particle-mesh algorithm with the ensemble Monte Carlo method for the simulation of ultra-small semiconductor devices," *IEEE Trans. Electron Devices*, vol. 47, no. 2, pp. 410–416, 2000, doi: 10.1109/16.822288.

[11] R. W.Hockney and J. W.Eastwood, *Computer simulation using particles*. New York: McGraw-Hill International Book Co., 1981.

[12] W. J.Gross, D.Vasileska, and D. K.Ferry, "Ultrasmall MOSFETs: the importance of the full Coulomb interaction on device characteristics," *IEEE Trans. Electron Devices*, vol. 47, no. 10, pp. 1831–1837, 2000, doi: 10.1109/16.870556.

[13] C.-Y.Cheng and D.Vasileska, "Electron transport analysis of 4H-SiC with full-band Monte Carlo simulation including real-space Coulomb interactions," *J. Appl. Phys.*, vol. 127, no. 15, p. 155702, 2020, doi: 10.1063/1.5144214.

[14] I. A.Khan and J. A.Cooper, "Measurement of High-Field Electron Transport in Silicon Carbide," *IEEE Trans. Electron Devices*, vol. 47, no. 2, pp. 269–273, 2000, doi: 10.1109/16.822266.

[15] J. B.Krieger and G. J.Iafrate, "Time evolution of Bloch electrons in a homogeneous electric field," *Phys. Rev. B*, vol. 33, no. 8, pp. 5494–5500, Apr.1986, doi: 10.1103/PhysRevB.33.5494.

[16] H. E.Nilsson, A.Martinez, and U.Sannemo, "Numerical study of Bloch electron dynamics in wide band-gap semiconductors," *Appl. Surf. Sci.*, vol. 184, no. 1–4, pp. 199–203, 2001, doi: 10.1016/S0169-4332(01)00503-7.

[17] R.Hathwar, M.Saraniti, and S. M.Goodnick, "Modeling of multi-band drift in nanowires using a full band Monte Carlo simulation," *J. Appl. Phys.*, vol. 120, no. 4, 2016, doi: 10.1063/1.4959881.